

This is the accepted manuscript made available via CHORUS. The article has been published as:

Proximity-Driven Enhanced Magnetic Order at Ferromagnetic-Insulator-Magnetic-Topological-Insulator Interface

Mingda Li, Cui-Zu Chang, Brian. J. Kirby, Michelle E. Jamer, Wenping Cui, Lijun Wu, Peng Wei, Yimei Zhu, Don Heiman, Ju Li, and Jagadeesh S. Moodera

Phys. Rev. Lett. **115**, 087201 — Published 17 August 2015

DOI: [10.1103/PhysRevLett.115.087201](https://doi.org/10.1103/PhysRevLett.115.087201)

Proximity Driven Enhanced Magnetic Order at Ferromagnetic Insulator / Magnetic Topological Insulator Interface

Mingda Li,^{1,2,3,*} Cui-Zu Chang,^{2,†} Brian. J. Kirby,⁴ Michelle Jamer,⁵ Wenping Cui,⁶ Lijun Wu,³ Peng Wei,² Yimei Zhu,³ Don Heiman,⁵ Ju Li,^{1,7} and Jagadeesh S. Moodera^{2,8,‡}

¹*Department of Nuclear Science and Engineering,
Massachusetts Institute of Technology, Cambridge, MA 02139, USA*

²*Francis Bitter Magnet Lab, Massachusetts Institute of Technology, Cambridge, MA 02139, USA*

³*Condensed Matter Physics and Materials Science Department,
Brookhaven National Laboratory, Upton, New York 11973, USA*

⁴*Center for Neutron Research, National Institute of Standards and Technology, Gaithersburg, Maryland 20899, USA*

⁵*Department of Physics, Northeastern University, Boston, MA 02115, USA*

⁶*Department of Physics, Boston College, Chestnut Hill, MA 02467, USA*

⁷*Department of Material Science and Engineering,
Massachusetts Institute of Technology, Cambridge, MA 02139, USA*

⁸*Department of Physics, Massachusetts Institute of Technology, Cambridge, MA 02139, USA*

(Dated: July 13, 2015)

Magnetic exchange driven proximity effect at a magnetic insulator / topological insulator (MI/TI) interface provides a rich playground for novel phenomena as well as a way to realize low energy dissipation quantum devices. Here we report a dramatic enhancement of proximity exchange coupling in the MI/magnetic-TI EuS / $\text{Sb}_{2-x}\text{V}_x\text{Te}_3$ hybrid heterostructure, where V doping is used to drive the TI (Sb_2Te_3) magnetic. We observe an artificial antiferromagnetic-like structure near the MI/TI interface, which may account for the enhanced proximity coupling. The interplay between the proximity effect and doping in a hybrid heterostructure provides insights into the engineering of magnetic ordering.

PACS numbers: 61.05.fj, 75.25.-j, 75.30.Gw, 75.70.Cn.

The time-reversal symmetry (TRS) breaking and surface bandgap opening of topological insulator (TI) is an essential step towards the observation of novel quantum phases and realization for TI-based devices [1, 2]. In general, there are two approaches to break the TRS: transitional metal (TM) ion doping [3–5] and magnetic proximity effect where a magnetic insulator (MI) adlayer induces exchange coupling [3, 6–8]. Doping TM impurities into TI will introduce a perpendicular ferromagnetic (FM) anisotropy and provide a straightforward means to open up the bandgap of TI's surface state, with profound influence to its electronic structure [4, 9–14]. In particular, quantum anomalous Hall effect (QAHE), where quantum Hall plateau and dissipationless chiral edge channels emerge at zero external magnetic field, has recently been realized in Cr-doped and V-doped TIs [9, 10, 15–20]. Ideally, compared to the doping method, proximity effect has a number of advantages, including spatially uniform magnetization, better controllability of surface state, freedom from dopant-induced scattering, as well as preserving TI intrinsic crystalline structure, etc. [21, 22]. However, due to the in-plane anisotropy and low Curie temperature, such MIs are usually too weak to induce strong proximity magnetism in TI. In fact, compared to magnetically doped TI which can induce as large as a 50 meV surface bandgap [4], the EuS/TI system has only 7 meV gap opening due to the strongly localized Eu-f orbitals [23]. Therefore, the enhancement of proximity magnetism is highly desirable to make it a valuable ap-

proach as doping hence takes full advantage.

In this *Letter*, we report significant enhancement of the proximity effect in MI EuS / magnetic-TI $\text{Sb}_{2-x}\text{V}_x\text{Te}_3$ hybrid heterostructure. Using polarized neutron reflectometry (PNR), we inferred an increase of proximity magnetization per unit cell (u.c.) in TI, from $1.2\mu_B/\text{u.c.}$ to $2.7\mu_B/\text{u.c.}$ at $x = 0.1$ doping level. High-resolution transmission electron microscopy (HRTEM) identifies the TI/EuS interfacial sharpness and excludes false positive magnetism signal from interdiffused Eu ions into TI. Furthermore, the proximity effect enhancement is accompanied by a decrease of the interfacial magnetization of EuS, resulting in an exotic antiferromagnetic (AF) structure. The existence of the “artificial” AF structure between FM EuS and the FM $\text{Sb}_{2-x}\text{V}_x\text{Te}_3$ is consistent with magnetometry measurements, and may shed light on creating artificial magnetic orders, such as AF structure reported here.

High-quality MI 6 nm EuS / 15 quintuple layer (QL) magnetic TI $\text{Sb}_{2-x}\text{V}_x\text{Te}_3$ hybrid heterostructures were grown by molecular beam epitaxy under a base vacuum $\sim 5 \times 10^{-10}$ Torr, where thin films $\text{Sb}_{2-x}\text{V}_x\text{Te}_3$ were grown on clean, heat-treated sapphire (0001) substrates with V-dopants coevaporated *in situ*. The EuS (111) layer was deposited *in situ* over the TI film using electron gun. To understand the interplay between proximity effect and TM doping, 6 nm EuS/ 15 QL Sb_2Te_3 , 15 QL $\text{Sb}_{2-x}\text{V}_x\text{Te}_3$ and 15 QL $\text{Sb}_{2-x}\text{V}_x\text{Te}_3$ samples were fabricated. The atomic configuration of the MI / magnetic

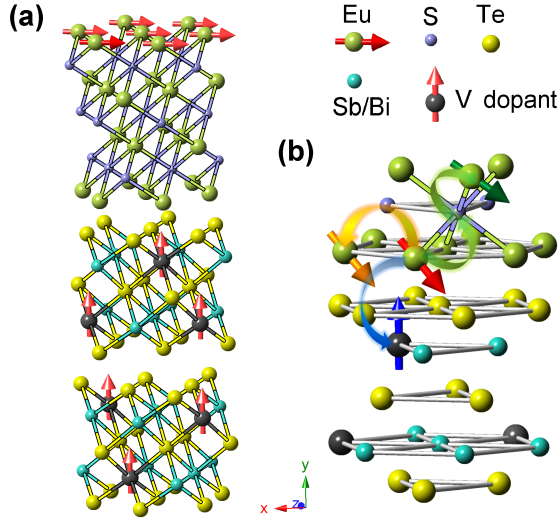


FIG. 1. (color). (a) MI EuS / V-doped TI Sb_2Te_3 hybrid heterostructure. The arrows denote the spin direction. The V-doped TI layer has a perpendicular magnetic anisotropy, while EuS has in-plane anisotropy. Such heterostructure may create an exotic magnetic environment near the interface, as illustrated in (b). For a given Eu ion (red-arrow), it interacts with neighborhood intra-plane Eu (orange-arrow) through Heisenberg interaction, inter-plane Eu ions (green-arrow) through super-exchange interaction, spin-polarized states at TI surface and localized moments in TI (blue-arrow).

TI heterostructure is shown in Fig. 1 (a). The EuS has in-plane anisotropy [24–27] within xz -plane, while the TM-doped TI has easy axis out-of-plane [10, 14, 20] along y -axis. The different anisotropy directions and a strong interfacial spin-orbit coupling create a complex magnetic environment for the interfacial EuS (Fig. 1 b). The Heisenberg interaction, superexchange interaction [25, 28], $d-f$ coupling [29] and coupling with the TI's spin texture may finally contribute to an overall augmentation of the proximity effect.

The PNR experiments were carried out using PBR beamline at the NIST-CNR, from which the in-plane magnetization is extracted. The experimental setup is shown in Fig. 2(a), where the incident spin-polarized neutrons are reflected by the sample, while the spin non-flip reflectivities from both spin components ($++$ and $--$) were collected under external guide magnetic field. The PNR refinement is based on a multilayered substrate / TI / proximity layer / interfacial EuS / main EuS model [22]. To maximize the PNR information extraction, we didn't compare the χ^2 with/without proximity effect due to limited sensitivity but presume the existence of the proximity coupling layer and optimize its magnitude.

The spin non-flip reflectivity curves for the main sample $\text{EuS}/\text{Sb}_{1.9}\text{V}_{0.1}\text{Te}_3$ and control sample $\text{EuS}/\text{Sb}_2\text{Te}_3$, at low (5 mT) and high (0.7 T) fields, are shown in Fig. 2 (b). The refinement of PNR is performed us-

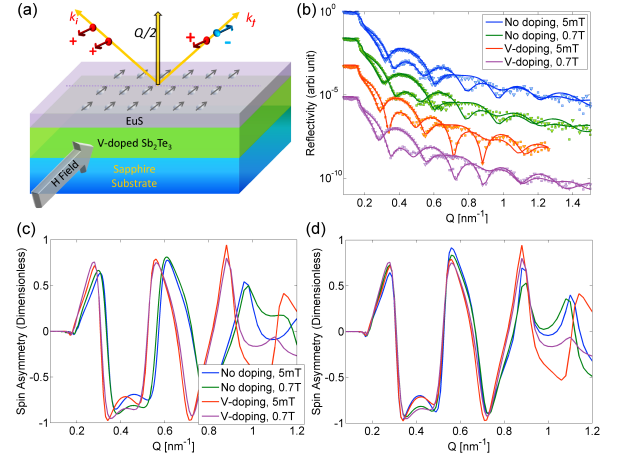


FIG. 2. (color). (a) The configuration of PNR. k_i , k_r and Q denote the incident, reflected and transferred wavevectors, respectively. (b) The spin + and spin - PNR data R^+ and R^- for the $\text{EuS}/\text{Sb}_{1.9}\text{V}_{0.1}\text{Te}_3$ and $\text{EuS}/\text{Sb}_2\text{Te}_3$ samples, at low (5 mT) and high (0.7 T) in-plane guide fields. The fitting results are represented by solid lines and shifted for clarity. (c) The spin asymmetry for the reflectivity in b. (d) The same spin asymmetry, but assuming control sample $\text{EuS}/\text{Sb}_2\text{Te}_3$ have exactly the same thickness as $\text{EuS}/\text{Sb}_{1.9}\text{V}_{0.1}\text{Te}_3$. In this way, the spin asymmetry difference is dominated by magnetic structure only. At $\sim 0.4 \text{ nm}^{-1}$, the difference comes from the effect of external magnetic field, while at $\sim 1.0 \text{ nm}^{-1}$ the difference mainly comes from V-dopants.

ing GenX [30]. To directly infer the possible contribution of V-dopants, the corresponding spin asymmetries $SA = \frac{R^+ - R^-}{R^+ + R^-}$ are plotted (Fig. 2c) for the raw and thickness-adjusted data (Fig. 2d). In this way, the different features of the SA in Fig. 2 (d) are solely coming from the magnetic structure since the crystalline structure is adjusted identical. We see that at $Q \sim 0.4 \text{ nm}^{-1}$, $\mu_0 H = 5 \text{ mT}$ SA for both samples with and without V-dopants overlap each other, but distinct with the $\mu_0 H = 700 \text{ mT}$ SA curves, indicating an effect from guide field; while at $Q \sim 1.0 \text{ nm}^{-1}$, a splitting of the SA curves for both samples at same guide field (eg. blue and red curves) is observed. This indicates the influence of the V-dopants to magnetic structure at high Q range (spatially localized) even without fitting.

The PNR results are shown in Fig. 3. The sapphire substrate lies in the region below 0 nm. Nuclear scattering length density (NSLD, red curves) identifies the compositional contrast, where the NSLDs for each layer are correctly reproduced from PNR fitting (sapphire substrate $5.5 \times 10^{-4} \text{ nm}^{-2}$, Sb_2Te_3 $1.8 \times 10^{-4} \text{ nm}^{-2}$, EuS $1.5 \times 10^{-4} \text{ nm}^{-2}$ and amorphous Al_2O_3 capping layer $4 \times 10^{-4} \text{ nm}^{-2}$), validating the fitting quality. In Fig. 3(a), without the EuS proximity layer, the V-dopants in the $\text{Sb}_{1.9}\text{V}_{0.1}\text{Te}_3$ sample contribute to $0.2 \mu_B/\text{u.c}$ in-plane magnetization at $\mu_0 H = 0.7 \text{ T}$, indicating a very strong perpendicular FM anisotropy. This is consistent

with the result in the inset of Fig. 4 (a), and facilitates us in obtaining reliable PNR refinement by fixing the magnetization of the magnetic TI layer. The magnetic SLD (MSLD, blue curves) at $\mu_0 H = 5\text{mT}$ and 700mT guide fields at $T = 5\text{K}$ are also plotted. In Fig. 3 (b), for the EuS/pure TI sample, we see a penetration of magnetization into TI, which is a direct signature of proximity magnetism. Unlike the EuS region where strong absorption SLD (ASLD) is always accompanied due to the Eu ions' extremely large neutron absorption cross section, the penetrated magnetization into TI does not show any absorption ($\sim 14 - 15\text{nm}$), indicating that such magnetism in TI is not from ferromagnetic Eu ions interdiffused into $\text{Sb}_{1.9}\text{V}_{0.1}\text{Te}_3$, but from proximity effect. The free of interdiffusion is also consistent with our TEM result in Fig. 3(d), where a sharp interface between epitaxially-grown EuS and $\text{Sb}_{1.9}\text{V}_{0.1}\text{Te}_3$ is developed.

The magnetization at the interface in proximity structures is greatly enhanced when V-dopants exist, from $1.2\mu_B/\text{u.c}$ (Fig. 3b, without V-doping) to $2.7\mu_B/\text{u.c}$ (Fig. 3c, V-doped). In both cases, the penetration depth of proximity is $\sim 1\text{nm}$, consistent with $\text{Bi}_2\text{Se}_3 / \text{EuS}$ interface [22]. Besides, the in-plane magnetization of EuS drops dramatically near the interface, from $\sim 3\mu_B/\text{u.c}$ without V-dopants to $\sim 0.5\mu_B/\text{u.c}$ with V-doping, at $\mu_0 H = 5\text{mT}$. This is due purely to magnetic effect instead of interfacial roughness since the ASLD is flat near the TI interface. On the contrary, magnetization drop at EuS / Al_2O_3 interface ($\sim 23\text{nm}$) is due to the Stran-ski-Krastanov growth [31], leading to a thickness variation and formation of island. This is directly confirmed from Z-contrast high-angle angular-dark-field (HAADF) HRTEM image (Fig. 3(d)). At higher field $\mu_0 H = 0.7\text{T}$, an increase of the in-plane EuS magnetism is accompanied with a drop of proximity effect into TI. Since only the perpendicular direction magnetism will contribute to the proximity effect [1], a high in-plane guide field tends to align the EuS moment in-plane and reduce the proximity.

To understand the origin of the drop of interfacial magnetism of EuS, we examined the exchange bias (EB) of the magnetic hysteresis measurements. Fig. 4 plots the results of low-field in-plane hysteresis measurements of a 2nm EuS / 10QL $\text{Bi}_{1.9}\text{V}_{0.1}\text{Te}_3$ hybrid heterostructure instead of Sb_2Te_3 since both belong to Bi_2Se_3 TI family and share very similar crystalline structure; Sb_2Te_3 is more suitable for PNR studies due to less interstitial V-defects, Bi_2Te_3 is better for SQUID due to higher diamagnetic susceptibility. Fig. 4(a, c) shows that the EB can be switched from negative to positive by a field $\mu_0 H = \pm 1\text{T}$, at 5K and 7K , respectively, where the corresponding EB and coercivity are plotted in Fig. 4(d). We adopt the traditional approach for EB measurement [32–34] at various resetting fields, where the EB was initially set negative by applying a field of -1T , followed by a positive field then measuring the low-field hysteresis [35]. This was re-

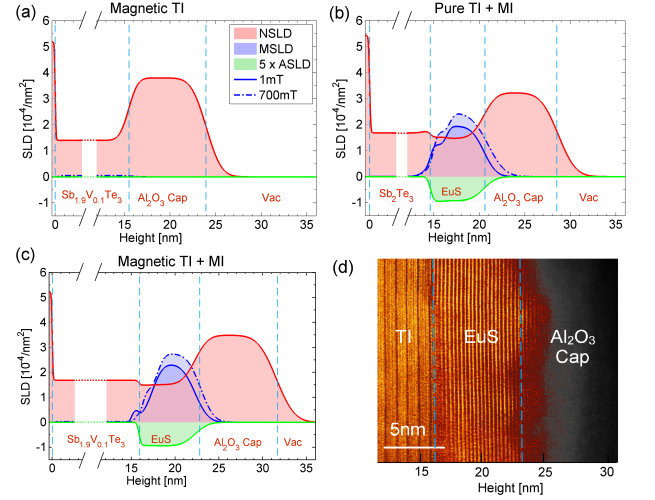


FIG. 3. (color). PNR fitting profiles of doping-only sample $\text{Sb}_{1.9}\text{V}_{0.1}\text{Te}_3$ (a), proximity-only sample $\text{EuS} / \text{Sb}_2\text{Te}_3$ (b) and hybrid heterostructure $\text{EuS}/\text{Sb}_{1.9}\text{V}_{0.1}\text{Te}_3$ (c). The NSLD, MSLD and ASLD denote the nuclear, magnetic and absorption scattering length density, which are measures of chemical contrast, magnetization and neutron absorption, respectively. The proximity effect is identified directly as finite magnetization signal (blue curves) in the region of TI near the TI/EuS interface ($\sim 15\text{nm}$). The absorption-free feature in this region excludes the possible contribution which solely comes from interdiffused Eu ions. We see clearly that with V-doping, the proximity magnetism is enhanced as a bump in (c), accompanied with a further suppression of magnetism of interfacial EuS ($15 - 18\text{nm}$). (d) HAADF TEM image of the $\text{EuS}/\text{Sb}_{1.9}\text{V}_{0.1}\text{Te}_3$ hybrid heterostructure. A sharp interface between the TI/MI is developed, indicating an epitaxial growth of EuS. This independent TEM result is quite consistent with (c) for uniformly distributed ASLD of EuS. The island-like crystalline facets between EuS and Al_2O_3 cap is also in very good agreement with the roughness in (c).

peated for resetting fields from 0 to $+0.8\text{T}$, where the bias is shifted from $H_{bias} = -5$ to $+6\text{Oe}$. Results of the exchange biasing strongly suggests the existence of an AF structure or possible magnetic frustration [36], and quite striking since our system is only composed of two strong FMs. The possible magnetic configuration is illustrated in Fig. 4(b), where V-doped TI keeps a perpendicular anisotropy, while interfacial AF structure is created to cause the EB.

To further understand the implication of the results in Fig. 4, we develop a phenomenological energy model to describe the AM/AF coupling. The anisotropic energy for bulk EuS can be written as [26]

$$E_{an} = \kappa_1 M_s t (\alpha_1^2 \alpha_2^2 + \alpha_1^2 \alpha_3^2 + \alpha_2^2 \alpha_3^2) + \kappa_2 M_s t \alpha_1^2 \alpha_2^2 \alpha_3^2 \quad (1)$$

where α_i is the directional cosine along i^{th} direction, M_s is the saturation magnetism per area, t is the thickness of FM layer and the anisotropic constants $\kappa_1 = -19.6\text{Oe}$ and $\kappa_2 = -4.6\text{Oe}$ at $T = 1.3\text{K}$ [26]. Since our interest is in thin film structures with a single symmetry axis (y -

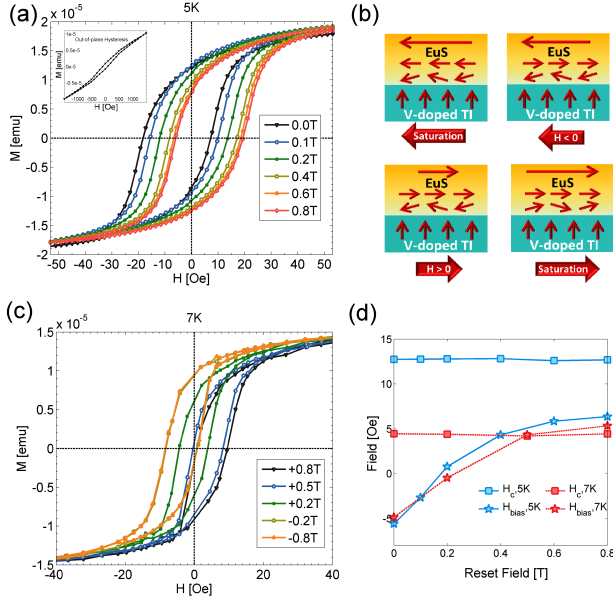


FIG. 4. (color). Magnetic measurements of a 2nm EuS / 10QL Bi_{1.9}V_{0.1}Te₃ hybrid heterostructure using a Quantum Design SQUID magnetometer. (a, c) In-plane hysteresis at 5K(a) and 7K(c), respectively, showing a negative EB following a set field of -1T which can be switched to positive bias by applying a positive resetting field. Inset of (a) is the out-of-plane magnetic hysteresis of the same sample, showing a finite remanent moment. (b) Schematic interfacial magnetic structure, where the interfacial EuS moments (horizontal arrows, the long arrow on the top of EuS means a saturated magnetization) are pinned by the exchange-coupled moments in the presence of V-doped TI (vertical arrows). (d) EB and coercive field as a function of the in-plane resetting field at 5K and 7K, respectively.

axis in Fig. 1 a), eq. (1) could be rewritten as using a simplified model for hexagonal and cubic lattice [37],

$$E_{an} = K_1 M_s t \sin^2(\theta) + K_2 M_s t \sin^4(\theta) \quad (2)$$

where $K_1 = \kappa_1 = -19.6$ Oe, $K_2 = -\frac{7}{8}\kappa_1 + \frac{1}{8}\kappa_2 = 16.6$ Oe, θ is the angle between the magnetization and the symmetry axis. Since $K_1 < 0$, $\theta = \pi/2$ corresponds in the present case for EuS showing easy-plane anisotropy within xz -plane. For a thin film, we further define $K_{1,eff} = K_s/t + K_1$. We require the surface anisotropy constant $K_s > 0$, since for thinner sample $K_{1,eff}$ will approach zero from the negative side, indicating a rotation of the in-plane easy plane to an out-of-plane direction, resulting in a magnetic canting which is reasonable for compensated thin film interfaces [33].

Taking into account the external magnetic field H and the FM/AF coupling J , the total energy could be written as

$$E = -H M_s t \sin(\theta) - J \sin(\theta) + \left(K_1 + \frac{K_s}{t}\right) M_s t \sin^2(\theta) + K_2 M_s t \sin^4(\theta) \quad (3)$$

TABLE I. Temperature dependence of the anisotropy constants. Green, Blue, red and black colored values are from [26], eq. (5), measurements in Fig.4 and eq. (4), respectively.

$T_c = 17$ K	1.3 K	5 K	7 K
K_1 (Oe)	-19.6	-13.10	-9.96
K_2 (Oe)	+16.6	7.41	4.29
H_c (Oe)	N/A	12.7	4.4
K_s/t (Oe)	13.8	9.3	7.2; 7.1

At saturation field configuration $\theta = \pm\pi/2$ and considering the energy extreme, we obtain the bias field and coercivity

$$H_{bias} = -\frac{J}{Mt}, \quad H_c = 2K_1 + 4K_2 + \frac{2K_s}{t} \quad (4)$$

respectively.

The anisotropic coefficients strongly depend on temperature [37]. In the mean-field approximation, the temperature dependence of anisotropy can be expressed using the Callen and Callen theory as [38]

$$K(T) = K(0) \left(1 - \frac{T}{T_c}\right)^{\frac{n(n+1)}{4}} \quad (5)$$

where n is the order of anisotropy constant, $n(K_1) = 2$ and $n(K_2) = 4$. Assuming that the Curie temperature of EuS is $T_c = 17$ K, we obtain the temperature dependence of anisotropy constants as shown in Table I. One remarkable feature for this model is that the surface anisotropy K_s/t calculated from experimental values and eq. (4) coincides with the independent check using eq. (5), giving 7.2 Oe vs 7.1 Oe at 7 K. Finally, this yields a surface anisotropy $K_s = 0.0014 \text{ erg} \cdot \text{cm}^{-2}$ by assuming a $2.5 \times 10^{-5} \text{ emu}$ saturation and 5 mm^2 sample area. This term is the origin of magnetic canting of interfacial EuS.

Contrary to the strong T -dependence of anisotropy, the bias field H_{bias} thus AF/FM coupling constant J has a weak dependence with temperature, indicating an origin of FM/AF coupling different from magnetic crystalline anisotropy such as the prominent role of spin-orbit interaction and spin-momentum locking at TI surface.

To summarize, we have reported a large enhancement of proximity exchange coupling strength in MI/magnetic-TI hybrid heterostructure. This overcomes the major disadvantage in MI/TI heterostructures where the proximity effect is considered weak [23]. To our knowledge, this is also the first report unionizing TM doping and proximity effect in MI. Here, the magnetic-TI with strong perpendicular anisotropy compensates the weakness of MI with in-plane anisotropy. Since energy gap of magnetic-TI at Γ point satisfies $E_g \propto M$ [39], when

treated as mean-field virtual crystal approximation, we have $M \propto x \propto T_C$ valid [40], where x is dopant concentration. In this regards, the interfacial magnetization enhancement implies increased energy gap hence increased working temperature of the interfacial magnetic order. The reduction of interfacial magnetism is consistent with the EB result, where an AF structure is artificially created, where a $K_s = 0.0014 \text{ erg} \cdot \text{cm}^{-2}$ surface anisotropy is extracted. Despite this value being small compared to the stronger examples such as the Au/Co interface [41], this approach provides fruitful insights to tailor new magnetic structure at TI/MI interfaces.

M. L. and C.Z.C. would thank the helpful discussion with Prof. Albert Fert. J.S.M. and C.Z.C. thank support from the STC CIQM under NSF grant DMR-1231319, NSF DMR grants 1207469 and ONR grant N00014-13-1-0301. M. J. and D. H. acknowledge support from NSF DMR-907007 and NSF ECCS-1402738. L.W. and Y.Z. were supported by DOE-BES under Contract No. DE-AC02-98CH10886.

* mingda@mit.edu

† czchang@mit.edu

‡ moodera@mit.edu

- [1] X.-L. Qi and S.-C. Zhang, *Reviews of Modern Physics* **83**, 1057 (2011).
- [2] M. Z. Hasan and C. L. Kane, *Reviews of Modern Physics* **82**, 3045 (2010).
- [3] P. Wei, F. Katmis, B. Assaf, *et al.*, *Physical Review Letters* **110**, 186807 (2013).
- [4] Y. Chen, J.-H. Chu, J. Analytis, *et al.*, *Science* **329**, 659 (2010).
- [5] M. Li, C.-Z. Chang, L. Wu, *et al.*, *Phys. Rev. Lett.* **114**, 146802 (2015).
- [6] M. Lang, M. Montazeri, M. C. Onbasli, Kou, *et al.*, *Nano Letters* **14**, 3459 (2014).
- [7] I. Vobornik, U. Manju, Fujii, *et al.*, *Nano letters* **11**, 4079 (2011).
- [8] A. Kandala, A. Richardella, D. W. Rench, *et al.*, .
- [9] C.-Z. Chang, W. Zhao, D. Y. Kim, *et al.*, *Nat Mater* **14**, 473 (2015).
- [10] C.-Z. Chang, J. Zhang, X. Feng, Shen, *et al.*, *Science* **340**, 167 (2013).
- [11] S.-Y. Xu, M. Neupane, C. Liu, *et al.*, *Nature Physics* **8**, 616 (2012).
- [12] Y. Hor, P. Roushan, H. Beidenkopf, *et al.*, *Physical Review B* **81**, 195203 (2010).
- [13] C.-Z. Chang, P. Tang, Y.-L. Wang, *et al.*, *Physical Review Letters* **112**, 056801 (2014).
- [14] C.-Z. Chang, J. Zhang, M. Liu, *et al.*, *Advanced Materials* **25**, 1065 (2013).
- [15] X.-L. Qi, T. L. Hughes, and S.-C. Zhang, *Physical Review B* **78**, 195424 (2008).
- [16] R. Yu, W. Zhang, H.-J. Zhang, *et al.*, *Science* **329**, 61 (2010).
- [17] C.-X. Liu, X.-L. Qi, X. Dai, *et al.*, *Physical Review Letters* **101**, 146802 (2008).
- [18] X. Kou, S.-T. Guo, Y. Fan, *et al.*, *Physical review letters* **113**, 137201 (2014).
- [19] J. Checkelsky, R. Yoshimi, A. Tsukazaki, *et al.*, *Nature Physics* **10**, 731–736 (2014).
- [20] C.-Z. Chang, P. Wei, and J. S. Moodera, *MRS Bulletin* **39**, 867 (2014).
- [21] M. Li, W. Cui, J. Yu, *et al.*, *Phys. Rev. B* **91**, 014427 (2015).
- [22] V. Lauter, F. Katmis, B. Assaf, and J. Moodera, in *APS March Meeting Abstracts*, Vol. W (2014) p. 42.00007.
- [23] S. Eremeev, V. Men'shov, V. Tugushev, *et al.*, *Physical Review B* **88**, 144430 (2013).
- [24] J. Kuneš and W. E. Pickett, *Physica B: Condensed Matter* **359**, 205 (2005).
- [25] L. Liu, *Solid State Communications* **46**, 83 (1983).
- [26] M. Franzblau, G. E. Everett, and A. Lawson, *Physical Review* **164**, 716 (1967).
- [27] S. Von Molnar and A. Lawson, *Physical Review* **139**, A1598 (1965).
- [28] W. Boncher, H. Dalafu, N. Rosa, and S. Stoll, *Coordination Chemistry Reviews* (2014).
- [29] V.-C. Lee and L. Liu, *Solid State Communications* **48**, 795 (1983).
- [30] M. Björck and G. Andersson, *Journal of Applied Crystallography* **40**, 1174 (2007).
- [31] A. Pimpinelli and J. Villain, *Physics of Crystal Growth* (Cambridge University Press, 1998) cambridge Books Online.
- [32] M. Kiwi, *Journal of Magnetism and Magnetic Materials* **234**, 584 (2001).
- [33] R. Stamps, *Journal of Physics D: Applied Physics* **33**, R247 (2000).
- [34] J. Nogués and I. K. Schuller, *Journal of Magnetism and Magnetic Materials* **192**, 203 (1999).
- [35] R. Wen-Bin, H. Mao-Cheng, Y. Biao, *et al.*, *Chinese Physics B* **23**, 107502 (2014).
- [36] C. Schlenker, S. Parkin, J. Scott, and K. Howard, *Journal of magnetism and magnetic materials* **54**, 801 (1986).
- [37] R. Skomski, *Simple models of magnetism* (Oxford University Press Oxford, 2008).
- [38] R. Skomski, O. Mryasov, J. Zhou, and D. J. Sellmyer, *Journal of applied physics* **99**, 08E916 (2006).
- [39] W. Luo and X.-L. Qi, *Phys. Rev. B* **87**, 085431 (2013).
- [40] W. Qin and Z. Zhang, *Phys. Rev. Lett.* **113**, 266806 (2014).
- [41] P. Bruno, *Journal of Physics F: Metal Physics* **18**, 1291 (1988).